NUCLEAR SCIENCE AND ENGINEERING
© 2019 American Nuclear Society
DOI: https://doi.org/10.1080/00295639.2019.1688087

Check for updates

Validation of Unresolved Neutron Resonance Parameters Using a Thick-Sample Transmission Measurement

Jesse M. Brown,[a]* R. C. Block,[a] A. Youmans,[a] H. Choun,[a] A. Ney,[a] E. Blain,[a] D. P. Barry,[b] M. J. Rapp,[b] and Y. Danon[a]

[a]*Rensselaer Polytechnic Institute, Department of Mechanical, Aerospace, and Nuclear Engineering, 110 8th Street, Troy, New York 12180*
[b]*Naval Nuclear Laboratory, P.O. Box 1072, Schenectady, New York 12301-1072*

Received October 1, 2019
Accepted for Publication October 26, 2019

Abstract — *Often discrepancies can be found in the corresponding cross sections of different evaluated nuclear data libraries. Traditional integral benchmarks that are used to validate such libraries are sensitive to cross-section values across many different energies. This means an erroneously low cross section at one energy may compensate for an erroneously high cross section at another energy, and the integral benchmark value may still be met. While the evaluated cross section may agree with that single benchmark, it could affect other systems differently. To reduce the potential for this error, an energy differential validation method is proposed herein for continuous energy Monte Carlo neutron transport models in the resolved resonance region and the unresolved resonance region (URR). The proposed method exposes the underlying physics of the URR and validates both the average cross section and resonance self-shielding effect driven by the fluctuations in that cross section. This is done by measuring the neutron transmission of a thick sample that, by its nature, exaggerates the resonance self-shielding effect. This validation method is shown to be very sensitive to the cross-section model used (resolved versus unresolved) and the fluctuation correction employed, allowing it to probe the validity of the previously mentioned cross-section evaluations. Tantalum-181 is used as an example to demonstrate the impact of different resonance evaluations. It was found that the JEFF-3.3 and JENDL-4.0u evaluations made reasonable choices for cross-section models of ^{181}Ta; none of the current evaluations, however, can be used to properly model the validation transmission over all energies. It was also found that updating resonance parameters in the URR provided better agreement with the validation transmission.*

Keywords — *Neutron transmission, validation nuclear data, unresolved resonance region, resonance parameters.*

Note — *Some figures may be in color only in the electronic version.*

I. INTRODUCTION

Tantalum is a chemically resistant[1] refractory metal with a high melting point[2] making it a desirable material for inhospitable environments such as nuclear power reactors. Tantalum is nearly monoisotopic, with an isotopic abundance of approximately 99.99% ^{181}Ta (Ref. 3). Though the neutron interaction cross section of tantalum has been measured in the past, few data have been reported in the energy region 0.2 to 100 keV, and the cross section in that region is not known with great detail. This energy region is especially important for next-generation reactors designed to operate with higher average neutron energies than today's thermal reactors as well as other applications with an intermediate neutron spectrum, such as those in which criticality safety is important. The lack of fine energy resolution data sets available for this isotope and the discrepancies found among evaluated libraries strongly motivate renewed investigation of the isotope ^{181}Ta.

*E-mail: brownjm@ornl.gov

Cross section is often classified into several different regions of energy, each with a corresponding semi-empirical model that best describes the physics of the region. There is a resolved resonance region (RRR) model for low energies, the unresolved resonance region (URR) model for energies just beyond the RRR, and the optical model in the fast or continuum region where the cross section varies slowly as a function of energy. Evaluations of ^{181}Ta in the ENDF/B-VIII.0 (Ref. 4), JEFF-3.3 (Ref. 5), and JENDL-4.0u (Ref. 6) libraries contain different parameters and methods to describe the RRR and URR, which result in inconsistent evaluated cross sections. The evaluated cross sections for the mentioned libraries are illustrated in Fig. 1.

JEFF-3.3 and JENDL-4.0u have nearly identical resonance parameters but differ in their treatment of the URR[a] whereas the ENDF/B-VIII.0 parameters deviate from the other two libraries significantly in the RRR and the URR. To validate which models should be used and where they should be used, experimental cross-section data and uncertainties on those data must be consulted. In the common ENDF-6 format, all of the previously mentioned libraries list the sources of the data for their evaluation. ENDF/B-VIII.0, JEFF-3.3, and JENDL-4.0u all list Mughabghab and Garber[7] and Macklin[8] for RRR and URR parameters; JENDL-4.0u (and by extension JEFF-3.3) lists that Yamamuro et al.[9] and Tsubone et al.[10] are also used.

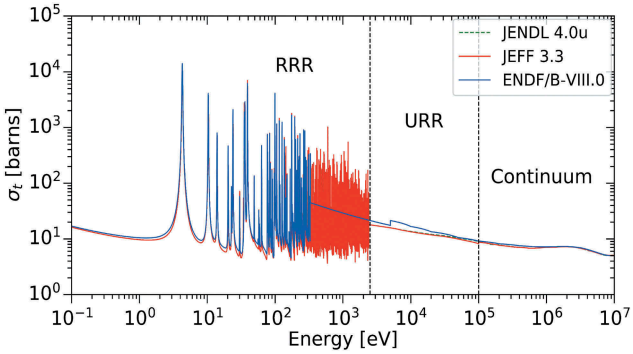

Fig. 1. The evaluated total cross sections σ_t from the JEFF-3.3, ENDF/B-VIII.0, and JENDL-4.0u libraries. The energy regions (RRR: 1 to 2400 eV, URR: 2.4 to 100 keV, and continuum: 0.1 to 10 MeV) are labeled by the model that is used to represent them in JEFF-3.3 and JENDL-4.0u. It can be seen that ENDF/B-VIII.0 deviates significantly from the other evaluations: ENDF/B-VIII.0 sets the end of the RRR at 330 eV and ends the URR model at 5 keV. The JEFF-3.3 and JENDL-4.0u libraries are nearly identical.

[a] JEFF-3.3 instructs users to reconstruct cross section based on the URR parameters listed in File 2 of the ENDF-6 format whereas JENDL-4.0u lists average cross section in File 3 of the ENDF-6 format. Both instruct to use the URR parameters listed in File 2 to correct for the resonance self-shielding effect. It should also be noted that JEFF-3.3 lists energy-dependent average parameters in the URR whereas JENDL-4.0u only allows the inelastic width to vary as a function of energy.

Among these references, the highest-resolution measurement is by Tsubone et al., who fit parameters up to 4.3 keV. Unfortunately, the Tsubone et al. transmission data and uncertainties are not publicly available. We are aware of only one high-resolution transmission data set, by Harvey et al.,[11] which provides data up to 3 keV. The Harvey et al. data set can be found on EXFOR (Ref. 12). The remaining publicly available total and capture cross section data sets contain a few measurements in the region of interest, which is 0.1 to 100 keV, but do not provide any information on the structure of the cross section in the energy region 0.3 to 30 keV. Without data that resolve structure in the kilo-electron-volt region, the impact of a new evaluation is limited. For this reason new measurements of ^{181}Ta have been made at Rensselaer Polytechnic Institute (RPI). An example of the total and capture cross-section data that are available on EXFOR (accessed 2018) are plotted in Fig. 2.

The validation method proposed in this work is similar to the high-energy transmission benchmarks of the past, which were typically in the mega-electron-volt range. Examples include the transmission measurements of Maerker and Muckenthaler,[21] Maerker,[22] and Murata et al.[23]; the spherical shell assemblies benchmarked by Janský[24] or Simakov et al.[25]; or the angular flux measurements of Malaviya et al.[26] Typically, in these experiments the differences in experimental and computed fluxes are compared. The transmission measurements in Refs. 21, 22, and 23 bear the closest resemblance to the present validation method but were focused on energies above the URR.

It is stressed here that the rapid fluctuations in cross sections must be properly accounted for when calculating transmission from cross section, or cross section from transmission. We sought to probe the validity of each of the evaluators' choices in cross-section models (and parameters used to describe them), with a focus on how fluctuations are treated. This was done by designing a transmission measurement that exaggerated the underlying physics in the URR and was sensitive to the models used in the RRRs and the URRs.

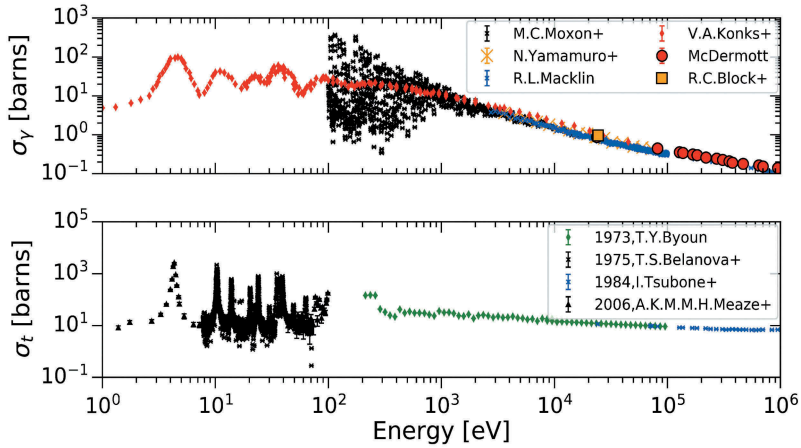

Fig. 2. A representative example of some of the available experimental total and capture cross-section data available on EXFOR for ^{181}Ta (accessed 2018). The + symbol following the author name in the legend indicates additional authors. Some error bars are not visible due to their size. Data sources are from Refs. 8, 9, and 13 through 20.

II. TOF CROSS-SECTION MEASUREMENTS

Neutron time-of-flight (TOF) experiments, such as those performed at the Gaerttner Linear Electron Accelerator (Linac) Center at RPI, provide a means for high-resolution, differential energy measurements. These include neutron transmission and neutron capture yield, which provide information necessary to calculate total cross section σ_t and capture cross section σ_γ, respectively. TOF measurements require knowledge of the time at which free neutrons are produced t_0 and the time at which a neutron interacts with the sample of interest or detection system t_i. The difference of these two quantities is defined as the TOF: $\text{TOF} = t_i - t_0$. The energy of a given neutron E is derived from the neutron TOF and some fixed flight path (FP) as

$$E_i = m_n c^2 \left(\frac{1}{\sqrt{1 - \frac{\left(\frac{\text{FP}}{t_i - t_0}\right)^2}{c^2}}} - 1 \right), \tag{1}$$

where m_n is the neutron mass and c is the speed of light in vacuum. At the RPI Linac this is achieved by colliding a very short pulse of electrons with a neutron-producing target and recording the moment t_0 at the time a bremsstrahlung gamma flash is produced from that target. These bremsstrahlung photons cause (γ, n) reactions in the target and produce a burst of neutrons in a range of energies. The highest-energy neutrons are around 50 MeV, and through neutron moderation the neutron energies can go to the thermal energy range. This gives the RPI Linac the capability to probe cross sections accurately over a large energy range.

II.A. Transmission

Neutron transmission measurements record the neutron count rate of a detector at some fixed FP for both a sample in the beam $\dot{C}_{Ta}(t_i)$ and no sample in the beam (open) $\dot{C}_o(t_i)$. The background subtracted ratio of these two quantities is the neutron transmission for the sample of interest:

$$T(t_i) = \frac{\dot{C}_{Ta}(t_i) - k_{Ta}\dot{B}(t_i) - \dot{B}0_{Ta}}{\dot{C}_o(t_i) - k_o\dot{B}(t_i) - \dot{B}0_o}. \tag{2}$$

The quantities $k_{Ta}\dot{B}(t_i)$ and $k_o\dot{B}(t_i)$ are the time-dependent backgrounds for the "sample in" and "open" measurements, respectively, normalized by their corresponding k_{Ta} and k_o. Respectively, $\dot{B}0_{Ta}$ and $\dot{B}0_o$ are the constant backgrounds for sample in and open. Usually, the quantity of interest is the total cross section, which is related to the transmission as

$$T(E) = e^{-n\sigma_t(E)}, \tag{3}$$

where n is the areal density of the sample in units of atoms per barn (at/b).

II.B. Resonance Self-Shielding

In all TOF measurements there is uncertainty in the neutron energy measured including, but not limited to, the time at which a neutron is emitted and detected and

the exact FP a neutron traveled. This uncertainty has the effect of broadening the observed transmission, which can effectively average out some of the fluctuations in the true cross section. This is the reason why a URR model is necessary, i.e., because resonance fluctuations are in the true unobserved cross section $\sigma_t(E)$ but cannot be observed due to the uncertainty in experiments. The following analysis will closely resemble that of Brown[27] and Semler.[28] The beginning of the URR for a measurement is often defined as where the uncertainty in TOF or E is greater than the spacing of the resonances. As all measurements are finite, the observed transmission or yield is always measured as an average over some finite energy. If the observable is transmission, the effective average transmission $\langle T \rangle$ is given by

$$\langle T(E) \rangle = \frac{\int_{E_1}^{E_2} \phi(E) e^{-n\sigma_t(E)} dE}{\int_{E_1}^{E_2} \phi(E) dE} \ . \tag{4}$$

For Eq. (4) the transmission is measured over some finite time bin with bin edges at times t_2 and t_1 that corresponds to the energy bin from E_1 to E_2. This energy bin determines the uncertainty in neutron energy $\Delta E = E_2 - E_1$. We shall assume that the flux $\phi(E)$ is constant in the energy range E_1 to E_2 and that the flux terms in the numerator and denominator cancel. After some manipulation,

$$\langle T(E) \rangle = \frac{1}{E_2 - E_1} \int_{E_1}^{E_2} e^{-n[\sigma_t(E) - \langle \sigma_t \rangle + \langle \sigma_t \rangle]} dE \ , \tag{5}$$

where $\langle \sigma_t \rangle$ is the total cross section averaged over the energy interval from E_1 to E_2. The average of the cross section $\langle \sigma_t \rangle$ in the energy bin E_1 to E_2 can be moved out of the integral as it is constant, and the final result is

$$\langle T(E) \rangle = e^{-n\langle \sigma_t \rangle} \left\{ \frac{1}{\Delta E} \int_{E_1}^{E_2} e^{-n[\sigma_t(E) - \langle \sigma_t \rangle]} dE \right\} \ . \tag{6}$$

Because of the nonlinear relationship of transmission and cross section, in general, $\langle T(\sigma_t(E)) \rangle \neq T(\langle \sigma_t(E) \rangle)$ (Ref. 29). If, however, the true unobserved cross section does not fluctuate away from the average cross section over the energy between E_1 and E_2, the bracketed term in Eq. (6) is nearly unity and $\langle T(\sigma_t(E)) \rangle \approx T(\langle \sigma_t(E) \rangle)$. It can also be deduced from Eq. (6) that if the sample areal density n (i.e., the sample optical thickness) is very small ($n\sigma_t << 1$), the bracketed term can again be driven more closely to unity.

This effect is often called the resonance self-shielding effect or perhaps more intuitively the transmission enhancement effect as the effective transmission is increased (effective cross section decreased) in thick self-shielded samples. To account for this fluctuation-driven resonance self-shielding effect, parameters in the RRR are used to predict the fluctuating behavior in the URR. This has been addressed in Monte Carlo neutron transport codes such as SESH (Ref. 30) and MCNP 6.1 (Ref. 31), which predict similar resonance self-shielding corrections.[13,32] In the MCNP 6.1 program, the probability table method is used, where cross-section probability distributions from NJOY21 (Ref. 33) are sampled. NJOY21 uses average resonance parameters to populate fictitious resonances. Sampled many times these fictitious resonances can, on average, properly predict the behavior of the cross section. This URR model and its evaluated parameters for ^{181}Ta are tested in this work with a validation transmission measurement, where the sample is chosen to be very thick ($n\sigma_t \geq 1$) to highlight the self-shielding effect.

The impact of the self-shielding correction is evident in Fig. 3. The self-shielding correction is determined by the ratio of corrected and uncorrected MCNP transmission calculations based on the evaluated JEFF-3.3 cross section. In the RRR there is no difference as MCNP only applies the correction to the average cross section in the URR. The transmission is corrected as much as 33% due to the resonance self-shielding effect for a 12-mm-thick sample of ^{181}Ta.

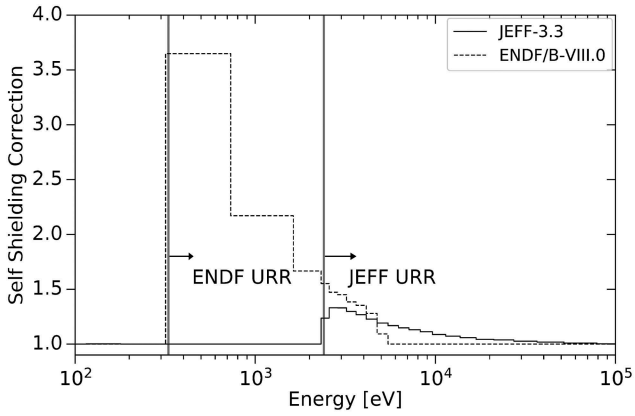

Fig. 3. The self-shielding correction as calculated by MCNP 6.1 for a 12-mm-thick sample of Ta. The correction factor is determined by the ratio of corrected and uncorrected MCNP transmission calculations based on the JEFF-3.3 evaluated cross section. In the RRR the correction is unity; this is due to the assumption that all fluctuations have been described by the model. The correction is greatest at the lowest-energy URR cross section as this region contained the greatest cross-section fluctuations. The correction for ENDF/B-VIII.0 changes the transmission by a factor as much as 3.5 for a 12-mm sample of Ta.

II.C. Resolution Boundary

For a single measurement the end of the RRR and the beginning of the URR can be defined by the location in energy space where the experimental uncertainty in neutron energy $\Delta E = D$, where D is the average energy spacing of the nuclear levels. This boundary between the RRR and the URR will be referred to as the resolution boundary. Upon consideration of many data sets with varying resolution, evaluators may use other metrics to determine where each model ought to be employed. A simple justification has often been made from the assumed linearity of the level spacing in the RRR. This is illustrated in Fig. 4.

The slope of the cumulative levels as a function of energy should be given by the inverse level spacing. Figure 4 shows that the cumulative levels and energy do not have a linear relationship for the entire energy range. It is assumed that the departure from linearity is caused by the experiment measuring an energy region where not all of the resonances are resolved. The resolution boundary can then be logically taken as the energy where nonlinearity begins. This is thought to be the reasoning behind the ENDF/B-VIII.0 choice of 330 eV for the resolution boundary. On the other hand, some evaluators have extended the RRR into the energy region where levels are clearly being missed, such as in the case of JEFF-3.3, to preserve the structure of the cross section better than the average used in the URR. The validation transmission method described herein is proposed as a way to determine the validity of the choices evaluators make for the resolution boundary.

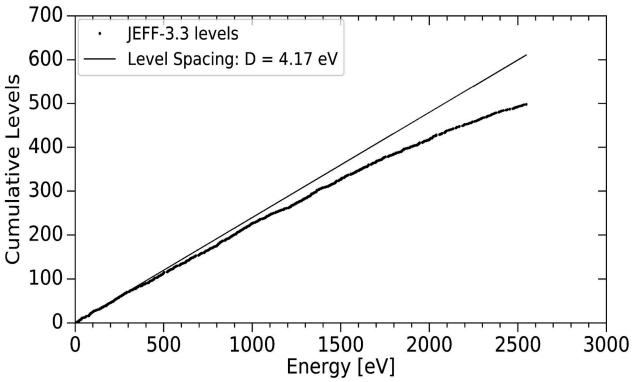

Fig. 4. The cumulative number of nuclear levels as a function of energy; in the RRR this relationship is assumed to be linear. The cumulative number of levels found in JEFF-3.3 is compared to the expected value given an average level spacing of $D = 4.17$ eV (Ref. 34). The departure from linearity is seen at approximately 300 eV. This nonlinearity could be caused by missing levels. ENDF/B-VIII.0 places the resolution boundary at 330 eV; JEFF-3.3 and JENDL-4.0u place the resolution boundary at 2400 eV. (Ref. 27.)

III. TRANSMISSION VALIDATION METHOD

III.A. Measurement

Evaluation choices made for the RRR and the URR models have impacts on the final predicted observables in continuous energy Monte Carlo codes such as MCNP. To validate the choices made in different evaluations, an accurate continuous energy validation measurement is required. The validating measurement was transmission through a 12-mm-thick Ta sample ($0.06716 \pm 0.21\%$ at/b) of 99.95% chemical purity. A depleted U sample (0.0821 at/b) was measured in tandem with the Ta to verify the background, a FP distance FP $= 35.18 \pm 0.04$ m, and $t_0 = 3.32 \pm 0.01$ μs. The sample dimensions and mass are listed for each of the two 6-mm samples stacked to create the 12-mm sample in Table I. In an effort to be explicit, the calculated quantities of density and areal density of the samples are listed as well. The sum of areal densities gives $n = 0.06716$ at/b for the 12-mm sample, and the quadrature sum of their corresponding uncertainties gives the 0.21% error on the 12-mm sample areal density. The sample impurities for the 12-mm Ta sample are listed in Table II and have units of parts per million (ppm).

The neutron source used was the RPI Linac with a neutron production target. The Linac was operated at 400 Hz with a 10-ns pulse width, a current of approximately 12 μA, and average electron beam energy of 55 MeV. The neutron detector used for the measurement was a 1.27-cm (0.5-in.)–thick glass doped with ^{6}Li viewed by two 12.7-cm (5-in.)–diameter photomultiplier tubes and placed along the east beamline. This detector is fully described by Barry in Ref. 35. The beam was

TABLE I

The Sample Dimensions of Each of the Two 6-mm Ta Samples

Dimension	6-mm Sample A	6-mm Sample B
Length (cm)	10.034 ± 0.001	10.022 ± 0.001
Width (cm)	10.0300 ± 0.0008	10.030 ± 0.001
Thickness (cm)	0.6064 ± 0.0013	0.6042 ± 0.0021
Mass (g)	1015.0 ± 0.1	1015.0 ± 0.1
ρ (g/cm^3)	16.63 ± 0.04	16.71 ± 0.06
n (at/b)	0.03356 ± 0.00007	0.03360 ± 0.00012

TABLE II

The Sample Impurities for the 12-mm Ta Sample

Element	Parts per Million	Element	Parts per Million
W	20	Nb	30
Mo	20	Ti	< 1
O	110	Al	< 1
N	20	Mn	< 1
C	20	Cu	< 1
H	8	Sn	< 1
Fe	20	Ca	< 5
Cr	3	Mg	< 1
Ni	3	Zr	< 1
Si	10		

collimated before and after the samples, which were placed at approximately 20 m from the neutron source. The majority of the beam path was under vacuum and contained fixed notches of 2.54-cm (1-in.)–thick Al and 0.0254-cm (0.01-in.)–thick Co as well as a 0.079375-cm (1/32-in.)–thick Cd overlap filter. The neutron production target consisted of a bare set of water-cooled Ta plates placed off the neutron beamline axis and a 2.54-cm (1-in.)–thick polyethylene disk placed on axis. This target is described in detail by Overberg et al.[36] as the bare bounce target (BBT). The measured count rate for the open beam ($\dot{C}_o$) and sample in ($\dot{C}_{Ta}$) configurations as well as their associated backgrounds ($k_o\dot{B}$,$k_{Ta}\dot{B}$) are shown in Fig. 5.

The configuration of the BBT has several advantages. The off-axis position of the Ta plates prevents a majority of the bremmstrahlung photons and Ta decay photons from reaching the neutron detector. The polyethylene disk used as a reflector also moderates the neutron spectrum, improving the signal-to-background ratio in the lower kilo-electron-volt energy region. The background is modeled by an exponential function with fitted parameters a and b as

$$\dot{B}(t_i) = a \cdot e^{-bt_i} + \dot{B}0 \ . \tag{7}$$

Equation (7) was fitted to the $\dot{B}0$ subtracted count rates at the 250-, 35-, 2.8-, and 0.132-keV resonances produced by Li, Al, Na, and Co samples, respectively. These samples were measured during separate dedicated background runs. This is referred to as the black resonance method, which has been used widely and its strengths and weaknesses have been discussed in detail by Syme.[37] This method of background treatment introduces

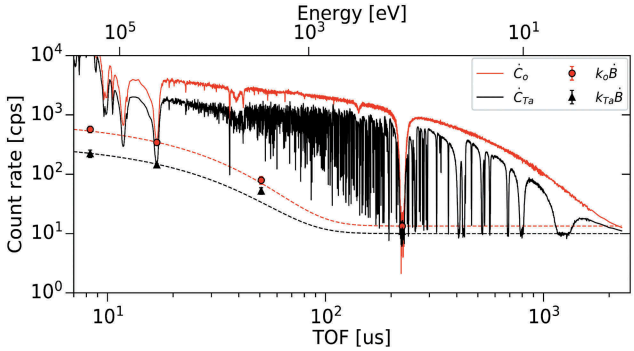

Fig. 5. The count rates for the thick Ta transmission. The experimental open and sample count rates are given by the red and black-dashed curves, respectively. Red and black circles and triangles indicate black resonance background count rates for the open and sample in count rates, respectively. The smooth red and black-dashed curves come from a function [Eq. (7)] fitted to the black resonance background points for the open and sample count rates, respectively. The statistical and systematic uncertainties from the background fit were propagated to the uncertainty in transmission. It should be noted that the errors on the black resonance count rates are too small to be visible.

correlations between the transmissions calculated for different time bins but contributes less than 2% uncertainty[b] across all energies.

The thickness of the Ta sample was chosen to amplify the effect of resonance self-shielding described in Sec. II.B. This measurement was designed to have a well-defined background with minimized in-beam photons and strong transmission enhancement due to resonance self-shielding. This resulted in a validation measurement that was very sensitive to the resonance parameters used in continuous energy Monte Carlo codes that model nuclear interactions.

The thick ^{181}Ta transmission measurement is shown in fine resolution along with the ^{238}U sample in Fig. 6. The transmission agrees relatively well with JEFF-3.3 in the low-energy RRR for the ^{181}Ta sample. It was assumed the RRR and the URR were well known for ^{238}U, and good agreement was found between the measured data and evaluation, verifying the data reduction of the ^{181}Ta.

III.B. Uncertainty and Correlation

The statistical uncertainty in the transmission was derived from the propagated uncertainties in the count

[b] Neglecting the uncertainty found at energies coinciding with Al resonances at 6, 35, and 88 keV where the count rate has been significantly reduced.

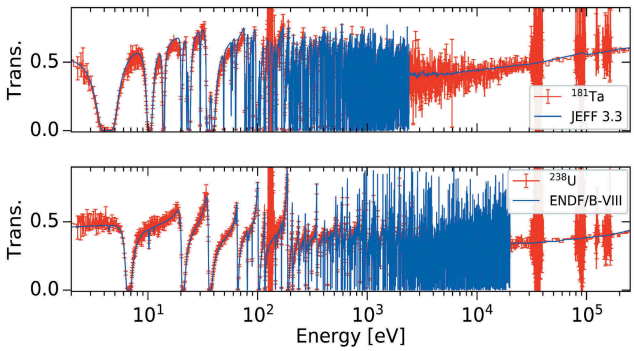

Fig. 6. The fine-resolution transmission for ^{181}Ta and ^{238}U compared to transmission for the evaluated JEFF-3.3 and ENDF/B-VIII.0 total cross sections, respectively. The ^{238}U sample was used to verify experimental parameters for the ^{181}Ta sample. Resonances in the fixed Al notch cause large variations in the transmission at approximately 35, 88, and 150 keV, as does the Co resonance at 132 eV. (Ref. 27.)

rates $\dot{C}_{Ta}(t_i), \dot{C}_O(t_i)$ and the background measurements that determined the black resonance count rates. The uncertainty in each time bin t_i was assumed to be independent of the other time bins in the TOF spectrum for the count rates. The fitted background and constant room background that were subtracted off of the count rates as seen in Eq. (2), however, introduce correlated uncertainty in the calculated $T(t_i)$ for different t_i. The background is a fit to black resonance count rates as described before. A least-squares fit was used to determine best fit parameters a and b and the associated uncertainty and correlation of each.

The relative neutron production rate from the neutron target is monitored periodically throughout the duration of the experiment by fission chambers at a short FP. The monitor count rates are then used to normalize each period of the experiment to a relative neutron rate to ensure the count rate is equivalent for both the sample and open measurement. To introduce the systematic uncertainty from the monitor normalization of count rates, Eq. (2) instead becomes

$$T(t_i) = \frac{\alpha_1 \dot{C}_{Ta}(t_i) - \alpha_2 k_{Ta} a e^{-bt_i} - \dot{B}0_{Ta}}{\alpha_3 \dot{C}_o(t_i) - \alpha_4 k_o a e^{-bt_i} - \dot{B}0_o}, \tag{8}$$

where the quantities $\alpha_{1,2,3,4}$ are nearly unity. The monitor normalization also introduces correlated error. The uncertainty on each of the monitors $\alpha_{1,2,3,4}$ is between 1%to2%. The uncertainty for k_{Ta} and k_o (4.3% and 5.5%, respectively) is derived from the normalization to the fixed Al notch count rate at 35 keV. To properly account for the correlated and uncorrelated uncertainties, an approach similar to that of Becker et al.[38] was employed. This method separates the propagation of the correlated and uncorrelated uncertainties and then adds the separate components to produce the $\mathrm{cov}(T_i, T_j) = \mathbf{C_y}$ as

$$\mathbf{C_y} = \mathbf{F_x C_x F_x}^T = \mathbf{F_{st} C_{st} F_{st}}^T + \mathbf{F_{sy} C_{sy} F_{sy}}^T. \tag{9}$$

In this notation the statistical (uncorrelated) uncertainty for $\dot{C}_{Ta}(t_i)$ and $\dot{C}_o(t_i)$ is contained in the diagonal elements of $\mathbf{C_{st}}$, and their associated Jacobian is $\mathbf{F_{st}}$. The systematic (correlated) uncertainty for $a, b, k_{Ta}, k_o, \dot{B}0_s, \quad \dot{B}0_o, \alpha_1, \alpha_2, \alpha_3,$ and α_4 is contained in the matrix $\mathbf{C_{sy}}$. The associated Jacobian for the systematic variables is contained in $\mathbf{F_{sy}}$. The sum of these two components is mathematically equivalent to the well-known uncertainty propagation equation,[39] given by the matrices with subscript $\mathbf{x}$. This method is documented in further detail in Ref. 27 along with the numerical results for the uncertainties and derivatives. The advantage of this separated method is the significant reduction in computation time and memory required. The full resulting covariance matrix $\mathbf{C_y}$ is transformed into a correlation matrix and plotted in Fig. 7 along with the transmission and fractional uncertainty therein.

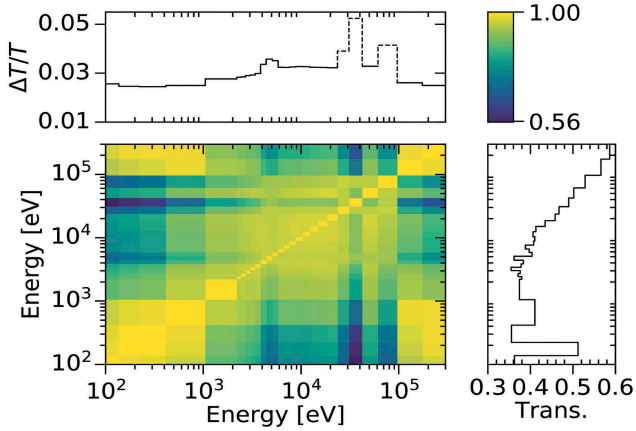

Fig. 7. The resultant energy-to-energy correlation matrix for transmission at each energy E_i. The transmission is plotted vertically on the right, and fractional uncertainty in the transmission is plotted at the top; the ordinate axis for each corresponds to the energy axes of the correlation matrix. As expected, the fractional uncertainty is greatest (indicated with dashed curves) where in-beam filter Al resonances occur: 35 and 88 keV. (Ref. 27.)

III.C. Results

To highlight the resonance self-shielding effect in the RRR and URR, the transmissions from the ^{181}Ta measurement and MCNP transmission calculations were grouped heavily and plotted together in Fig. 8. The fine-resolution transmissions from the experiment and libraries were grouped in the same manner. The grouping scheme was designed so that each energy bin would include a significant number of resonances; in this case each bin was designed to include 50 or more. Transmission as predicted by the JENDL-4.0u evaluation has not been included in the plot as it did not deviate significantly from the JEFF-3.3 transmission in the energy range of interest.

It was seen from 200 to 2400 eV that the JEFF-3.3 evaluation could be used to model the measurement much better than ENDF/B-VIII.0 by simply extending the RRR to 2400 eV. The extension of the RRR in the JEFF-3.3 evaluation was not negatively affected by missing levels. This is likely due to the small size of the missing levels, which would cause insignificant self-shielding. The JEFF-3.3 evaluation also extends the URR to 100 keV, as compared to the ENDF/B-VIII.0 evaluation stopping at 5 keV. This extension of the URR enables a fluctuation correction much higher, which is seen to be important.

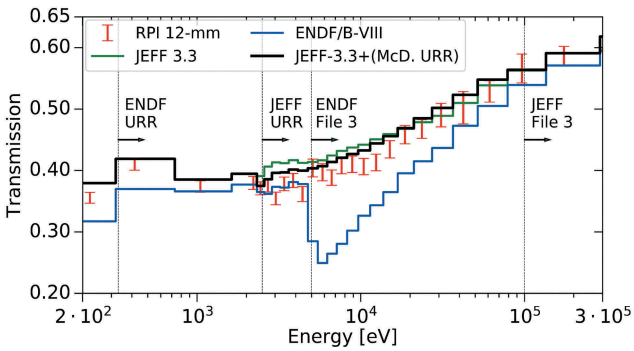

Fig. 8. Transmission of a 12-mm ^{181}Ta sample was measured at the RPI Linac and compared to MCNP simulations of transmission using JEFF-3.3, ENDF/B-VIII.0, and a modified JEFF-3.3 file with RPI average parameters from McDermott et al.[13] The RPI modification only changed the resonance parameters in the URR. It can be seen from 200 to 2400 eV that the JEFF-3.3 evaluation performs better than ENDF/B-VIII.0 simply by extending the RRR. ENDF/B-VIII.0 does not account for any fluctuation in the cross section beyond 5 keV as it draws from File 3. The greatest discrepancy between JEFF-3.3 and the validation transmission can be seen in the URR from 2 to 25 keV. The URR discrepancy becomes less significant as energy increases and cross-section fluctuations decrease. (Ref. 27.)

The strong dip in the ENDF/B-VIII.0 transmission at 5 keV is largely due to the transition from File 2 (URR model) to File 3 (average cross section) at that energy. The File 3 cross section does not contain any information to account for self-shielding. The most glaring discrepancy between JEFF-3.3 and the validation transmission is seen from approximately 2 to 25 keV.

III.D. Improvements

To investigate the discrepancy between JEFF-3.3 and the validation transmission, recent capture measurements from RPI were consulted. McDermott et al.[13] made a capture measurement of ^{181}Ta at RPI using a filtered beam technique. The filtered beam technique is a measurement with high signal-to-background ratio, and the McDermott et al. results agree with other trusted capture measurements of Ta such as that of Wisshak et al.[40] The McDermott et al. measurement generated capture yield from approximately 24 keV to 1 MeV, and average resonance parameters for the region were reported. These average parameters were used to create URR parameters in the ENDF/B format to replace those of JEFF-3.3. A comparison of various average level parameters used to describe the URR from 24 keV to 1 MeV is given in Table III.

The JEFF-3.3 ENDF file was modified by replacing JEFF-3.3 average parameters in the URR; nothing else was changed. This file was then used to generate the A Compact ENDF (ACE) file using NJOY2021. The ACE file is the data input for MCNP, which was again used to simulate the neutron transmission experiment performed at RPI. The results of the RPI-modified JEFF-3.3 ENDF/B file are shown in Fig. 8.

Here, it can be seen that the resulting calculation reduces the discrepancies found in the energy range 2 to 25 keV. This is partly due to the reduced level spacing used in the URR. The RPI modification reduced the level spacing to that found in *Atlas of Neutron Resonances* by Mughabhgab, resulting in less resonance fluctuation in the URR. This reduction in predicted resonance fluctuation results in a reduced transmission in the RPI modification compared to JEFF-3.3. The structured nature of the cross section, however, still remains unaccounted for. It should be noted that the McDermott et al. evaluated parameters come from fitting the experimental capture cross section and the theoretical JEFF-3.2 total cross section, biasing the evaluation to JEFF-3.2. This can be improved by making URR transmission measurements and including them in the fit; this is important for predicting an accurate cross section for ^{181}Ta in the URR.

TABLE III

Various Average Level Parameters Used to Describe the URR*

Parameters	McDermott et al.	*Atlas of Neutron Resonances*	JEFF-3.3
$S_0 \times 10^4$	1.71 ± 0.12	1.74 ± 0.12	1.7
$S_1 \times 10^4$	0.52 ± 0.10	0.5 ± 0.2	0.2
$S_2 \times 10^4$	2.60 ± 0.60	2.3 ± 0.3	2.3
$\langle \Gamma_{\gamma,0} \rangle$ (meV)	62.6 ± 5.1	60.5 ± 2.0	65.0
$\langle \Gamma_{\gamma,1} \rangle$ (meV)	55.0 ± 13.1	n/a[a]	n/a
$\langle \Gamma_{\gamma,2} \rangle$ (meV)	62.6 ± 5.1	n/a	n/a
D (eV)	$4.17 \pm 0.04^{\dagger}$	4.17 ± 0.04	n/a
$R_0^{\infty} \times 10^3$	41 ± 20	n/a	n/a
$R_1^{\infty} \times 10^3$	13 ± 19	n/a	n/a
$R_2^{\infty} \times 10^3$	18 ± 11	n/a	n/a
R' (fm)	7.67 ± 0.08	7.6 ± 0.2	7.8
a_c (fm)	7.92	n/a	n/a

*The average parameters from McDermott et al. are listed as well as the average parameters found in *Atlas of Neutron Resonances*[34] by Mughabghab. McDermott et al. used the average level density of Mughabghab, as indicated by the †. The information header of the ENDF/B file in the JEFF-3.3 evaluation takes average parameters used for the URR from JENDL-4.0u, where parameters are listed without any associated uncertainties. Subscripts indicate quantum angular momentum for $l = 0, 1, 2$.
[a]n/a = not applicable.

IV. CONCLUSION

A sensitive measurement that exposes the underlying physics of the URR was designed and executed to validate resonance evaluations in the RRR and the URR. This validation method is an effective tool for evaluators that provides excellent feedback regarding resonance self-shielding and whether extension of the RRR is or is not justified. It was found that the JEFF-3.3 evaluation made mostly reasonable assumptions for resonance parameters and modeling of the RRR and the URR. Extending the RRR beyond the energy where levels are being missed has been shown to improve modeling of the cross section for ^{181}Ta. This is seen in the differences of the JEFF-3.3 and ENDF/B-VIII.0 transmissions between energies 330 eV and 2.4 keV. The region in which average parameters are calculated from the RRR for the URR, however, must be carefully chosen based on where measurements resemble well-known distributions of nuclear physics. The validation transmission also shows that the ENDF/B-VIII.0 cross-section representation would benefit from extending the URR to as much as 100 keV. Our preliminary resonance parameters and evaluation choices result in an MCNP calculation that outperforms JEFF-3.3 and ENDF/B-VIII.0 for the transmission validation in the URR. The thick sample differential transmission measurement as described herein could be used to supplement and improve existing integral benchmarks in the process of validating resonance parameter evaluations.

Acknowledgments

We wish to thank Peter Brand, Michael Bretti, Azeddine Kerdoun, Larry Krusieski, and Matt Gray for their skillful operation of the RPI Linac and diligent support with mechanical and electrical work. We also thank Brian Epping. This work was sponsored by the U.S. Department of Energy, Nuclear Criticality Safety Program.

ORCID

Jesse M. Brown http://orcid.org/0000-0002-0769-4100
Y. Danon http://orcid.org/0000-0001-6187-9731

References

1. D. F. TAYLOR, "Acid Corrosion Resistance of Tantalum, Columbium, Zirconium, and Titanium," *Ind. Eng. Chem.*, **42**, *4*, 639 (1950); https://doi.org/10.1021/ie50484a023.
2. L. MALTER and D. LANGMUIR, "Resistance, Emissivities and Melting Point of Tantalum," *Phys. Rev.*, **55**, *8*, 743 (1939); https://doi.org/10.1103/PhysRev.55.743.
3. M. WEISER et al., "Atomic Weights of the Elements 2011," *Pure Appl. Chem.*, **85**, *5*, 1047 (2013).
4. D. BROWN et al., "ENDF/B-VIII.0: The 8th Major Release of the Nuclear Reaction Data Library with CIELO-Project Cross Sections, New Standards and Thermal Scattering Data," *Nucl. Data Sheets*, **148**, 1 (2018); https://doi.org/10.1016/j.nds.2018.02.001.

5. "The JEFF-3.3 Evaluated Data Library," Organisation for Economic Co-operation and Development Nuclear Energy Agency (2017); https://www.oecd-nea.org/dbdata/jeff/jeff33/index.html#neutron (current as of Dec. 27, 2018).
6. K. SHIBATA and J. KATAKURA, "JENDL-4.0: A New Library for Nuclear Science and Engineering," *J. Nucl. Sci. Technol.*, **48** (2011); https://doi.org/10.1080/18811248.2011.9711675.
7. S. F. MUGHABGHAB and D. I. GARBER, "Neutron Cross Sections, Volume 1, Resonance Parameters," BNL 325, Brookhaven National Laboratory (1973).
8. R. L. MACKLIN, "Neutron Capture Cross Sections of Tantalum from 2.6 To 1900 keV," *Nucl. Sci. Eng.*, **86**, *4*, 362 (1984); https://doi.org/10.13182/NSE84-A18637.
9. N. YAMAMURO et al., "Neutron Capture Cross Section Measurements of Nb-93, I-127, Ho-165, Ta-181, and U-238 Between 3.2 and 80 keV," *J. Nucl. Sci. Technol.*, **17**, *8*, 582 (1980); https://doi.org/10.1080/18811248.1980.9732628.
10. I. TSUBONE, Y. NAKAJIMA, and Y. KANDA, "Resonance Parameters of Tantalum-181 in Neutron Energy Range from 100 to 4300 eV," *J. Nucl. Sci. Technol.*, **24**, *12*, 975 (1987); https://doi.org/10.1080/18811248.1987.9733533.
11. J. HARVEY et al., "High-Resolution Neutron Transmission Measurements on ^{235}U, ^{239}Pu, and ^{238}U," Oak Ridge National Laboratory (1988).
12. N. OTUKA et al., "Towards a More Complete and Accurate Experimental Nuclear Reaction Data Library (EXFOR): International Collaboration Between Nuclear Reaction Data Centres (NRDC)," *Nucl. Data Sheets*, **120**, 272 (2014); https://doi.org/10.1016/j.nds.2014.07.065.
13. B. J. McDERMOTT et al., "^{181}Ta(n, γ) Cross Section and Average Resonance Parameter Measurements in the Unresolved Resonance Region from 24 to 1180 keV Using a Filtered-Beam Technique," *Phys. Rev. C*, **96**, 014607 (2017); https://doi.org/10.1103/PhysRevC.96.014607.
14. M. MOXON and E. RAE, "A Gamma Ray Detector for Neutron Capture Cross Section Measurements," *Nucl. Instrum. Meth.*, **24**, 445 (1963); https://doi.org/10.1016/0029-554X(63)90364-1.
15. V. KONKS, Y. P. POPOV, and F. SHAPIRO, "Cross Sections for Radiative Capture of Neutrons with Energies up to 50 keV by ^{139}La, ^{141}Pr, ^{181}Ta, and ^{197}Au Nuclei," *Zh. Ehksp. Teor. Fiz.*, **46** (1964).
16. R. BLOCK, N. KAUSHAL, and R. HOCKENBURY, "Iron-Filtered Neutron Beams: A New Approach to Precision Time-of-Flight Cross Section Measurements," Rensselaer Polytechnic Institute (1972).
17. I. TSUBONE et al., "Neutron Total Cross Sections of ^{181}Ta and ^{238}U from 24.3 keV to 1 MeV and Average Resonance Parameters," *Nucl. Sci. Eng.*, **88**, *4*, 579 (1984); https://doi.org/10.13182/NSE84-A18374.
18. T. S. BELANOVA et al., "Neutron Resonances in ^{181}Ta at 2–70 eV," *Sov. At. Energy*, **38**, *6*, 553 (1975); https://doi.org/10.1007/BF01127449.
19. K. YOO et al., "Measurements of the Neutron Total Cross-Sections of Tantalum by Using Pulsed Neutrons Based on an Electron Linac," *J. Korean Phys. Soc.*, **48**, *4*, 827 (2006).
20. T. Y. BYOUN, "Experimental Investigation of the Resonance Self-Shielding and Doppler Effect in Uranium and Tantalum," No. 3058-34, Prog: Chicago Operations Office, A.E.C., Contract Report (1973).
21. R. MAERKER and F. MUCKENTHALER, "Final Report on a Benchmark Experiment for Neutron Transport Through Iron and Stainless Steel," Oak Ridge National Laboratory (1974).
22. R. MAERKER, "SDT1. Iron Broomstick Experiment: An Experimental Check of Neutron Total Cross Sections," Oak Ridge National Laboratory (1972).
23. I. MURATA et al., "Neutron–Nuclear Data Benchmark for Copper and Tungsten by Slab Assembly Transmission Experiments with DT Neutrons," *Fusion Eng. Des.*, **58**, 617 (2001); https://doi.org/10.1016/S0920-3796(01)00518-X.
24. B. JANSKÝ et al., "Mixed Neutron and Gamma Spectra Measurements and Calculations in Pure Iron Benchmark Assembly with Cf-252 Neutron Source," *J. Nucl. Sci. Technol.*, **39**, *sup2*, 1033 (2002); https://doi.org/10.1080/00223131.2002.10875278.
25. S. P. SIMAKOV et al., "Benchmarking of Evaluated Neutron Data for Vanadium by a 14 MeV Spherical Shell Transmission Experiment," International Atomic Energy Agency (1998).
26. B. MALAVIYA et al., "Experimental and Analytical Studies of Fast Neutron Transport in Iron," *Nucl. Sci. Eng.*, **47**, *3*, 329 (1972); https://doi.org/10.13182/NSE72-A22419.
27. J. M. BROWN, " Measurements, Evaluation, and Validation of Ta-181 Resolved and Unresolved Resonance Regions," Doctoral Thesis, Rensselaer Polytechnic Institute (2019).
28. T. T. SEMLER, "Analysis of Temperature-Dependent Neutron Transmission and Self-Indication Measurements on Tantalum at 2-keV Neutron Energy," NASA TN D-7214, National Aeronautics and Space Administration, Lewis Research Center (1973).
29. J. L. W. V. JENSEN, "Sur les fonctions convexes et les inegalites entre les valeurs moyenne," *Acta Math.*, **30**, 175 (1906); https://doi.org/10.1007/BF02418571.
30. F. FRÖHNER, "SESH—A FORTRAN IV Code for Calculating the Self-Shielding and Multiple Scattering Effects for Neutron Cross Section Data Interpretation in

the Unresolved Resonance Region," Gulf General Atomic, Inc. (1968).

31. T. GOORLEY et al., "Initial MCNP6 Release Overview," *Nucl. Technol.*, **180**, 298 (2012); https://doi.org/10.13182/NT11-135.
32. R. BAHRAN et al., "Isotopic Molybdenum Total Neutron Cross Section in the Unresolved Resonance Region," *Phys. Rev. C*, **92**, 024601 (2015); https://doi.org/10.1103/PhysRevC.92.024601.
33. R. MacFARLANE et al., "The NJOY Nuclear Data Processing System, Version 2016," LA-UR-17-20093, Los Alamos National Laboratory; https://doi.org/10.2172/1338791 (2017).
34. S. MUGHABGHAB, *Atlas of Neutron Resonances*, Elsevier, Oxford (2006).
35. D. P. BARRY, "Neodymium Neutron Transmission and Capture Measurements and Development of a New Transmission Detector," Doctoral Thesis, Rensselaer Polytechnic Institute (2003).
36. M. OVERBERG et al., "Photoneutron Target Development for the RPI Linear Accelerator," *Nucl. Instrum. Meth. Phys. Res. A*, **438**, *2*, 253 (1999); https://doi.org/10.1016/S0168-9002(99)00878-5.
37. D. SYME, "The Black and White Filter Method for Background Determination in Neutron Time-of-Flight Spectrometry," *Nucl. Instrum. Meth. Phys. Res.*, **198**, *2*, 357 (1982); https://doi.org/10.1016/0167-5087(82)90276-9.
38. B. BECKER et al., "Data Reduction and Uncertainty Propagation of Time-of-Flight Spectra with AGS," *J. Instrum.*, **7**, *11*, P11002 (2012); https://doi.org/10.1088/1748-0221/7/11/p11002.
39. K. ARRAS, "An Introduction to Error Propagation: Derivation, Meaning and Examples of Equation $C_y = F_x C_x F_x^T$," EPFL-ASL-TR-98-01 R3, Ecole Polytechnique Federale de Lausanne (1998).
40. K. WISSHAK et al., "Measurements of keV Neutron Capture Cross Sections with a 4π Barium Fluoride Detector: Examples of ^{93}Nb, ^{103}Rh, and ^{181}Ta," *Phys. Rev. C*, **42**, 1731 (1990); https://doi.org/10.1103/PhysRevC.42.1731.